Cell

CAPS-1 and CAPS-2 Are Essential Synaptic Vesicle Priming Proteins

Wolf J. Jockusch,[1] Dina Speidel,[1,3] Albrecht Sigler,[2,4] Jakob B. Sørensen,[2] Frederique Varoqueaux,[1] Jeong-Seop Rhee,[1,*] and Nils Brose[1,*]

[1]Max Planck Institute of Experimental Medicine, Department of Molecular Neurobiology, Hermann-Rein-Str. 3, D-37075 Göttingen, Germany

[2]Max Planck Institute of Biophysical Chemistry, Department of Membrane Biophysics, Am Faßberg 11, D-37077 Göttingen, Germany

[3]Present address: Lund University, Department of Clinical Sciences Malmö, UMAS Ing 72, CRC 91-11, S-20502 Malmö, Sweden.

[4]Present address: University of British Columbia, Kinsman Laboratory of Neurological Research, 2255 Wesbrook Mall, Vancouver, V6T 1Z3, Canada.

*Correspondence: rhee@em.mpg.de (J.-S.R.), brose@em.mpg.de (N.B.)

DOI 10.1016/j.cell.2007.11.002

SUMMARY

Before transmitter-filled synaptic vesicles can fuse with the plasma membrane upon stimulation they have to be primed to fusion competence. The regulation of this priming process controls the strength and plasticity of synaptic transmission between neurons, which in turn determines many complex brain functions. We show that CAPS-1 and CAPS-2 are essential components of the synaptic vesicle priming machinery. CAPS-deficient neurons contain no or very few fusion competent synaptic vesicles, which causes a selective impairment of fast phasic transmitter release. Increases in the intracellular Ca^{2+} levels can transiently revert this defect. Our findings demonstrate that CAPS proteins generate and maintain a highly fusion competent synaptic vesicle pool that supports phasic Ca^{2+} triggered release of transmitters.

INTRODUCTION

Synaptic transmission is triggered by SNARE-mediated fusion of synaptic vesicles (SVs). Typically, only primed SVs can fuse with the plasma membrane upon stimulation. The underlying priming reaction is essential for synaptic transmission (Augustin et al., 1999; Varoqueaux et al., 2002). Its regulation determines synaptic strength and short-term plasticity, which in turn controls many important brain functions ranging from sensory adaptation to sound localization and cortical gain control (Junge et al., 2004; Rhee et al., 2002). SV priming is dependent on members of the Munc13/Unc-13 family of presynaptic active zone proteins (Varoqueaux et al., 2002), which regulate the t-SNARE Syntaxin (Betz et al., 1997; Gracheva et al., 2006; McEwen et al., 2006; Richmond et al., 2001; Stevens et al., 2005). αRIMs, which anchor and regulate Munc13s at synapses, modulate SV priming (Andrews-Zwilling et al., 2006; Betz et al., 2001; Dulubova et al., 2005). Apart from Munc13s and αRIMs, the components of the SV priming machinery are unknown, and its molecular mode of action has remained elusive.

CAPS-1 and CAPS-2 are candidate vesicle priming proteins as they contain a sequence stretch with homology to the priming domain of Munc13s (Basu et al., 2005; Koch et al., 2000; Stevens et al., 2005). CAPS-1 is thought to be a specific regulator of large dense-core vesicle (LDCVs) fusion (Rupnik et al., 2000; Sadakata et al., 2007, 2004; Speese et al., 2007; Tandon et al., 1998), although SV and LDCV secretion processes have many features and most other protein components in common (Morgan and Burgoyne, 1997). CAPS-1 was initially discovered as a regulator of Ca^{2+}-triggered LDCV fusion (Walent et al., 1992). Subsequent studies on brain synaptosomes and on synaptic transmission in *C. elegans* mutants lacking the CAPS homolog Unc-31 indicated that CAPS-1/Unc-31 might specifically regulate LDCV but not SV exocytosis (Gracheva et al., 2007; Speese et al., 2007; Tandon et al., 1998). SV fusion at *Drosophila* neuromuscular synapses is reduced in mutants lacking the CAPS homolog Unc-31, but this phenotype was interpreted to be the consequence of a primary defect in LDCV secretion (Renden et al., 2001). Similarly, *C. elegans unc-31* mutants exhibit uncoordinated locomotor activity and reduced neuromuscular synaptic transmission, but this phenotype was also interpreted to result from an indirect effect of altered LDCV function (Gracheva et al., 2007; Speese et al., 2007). CAPS-1 deletion mutant mice exhibit perturbations of catecholamine uptake into LDCVs and of LDCV fusion (Speidel et al., 2005), and deletion of CAPS-2 in mice causes abnormal cerebellar development and short-term synaptic plasticity (Sadakata et al., 2007).

Essentially, all currently available data would be compatible with the current model of an LDCV-specific role of CAPS proteins. However, CAPS-1 and CAPS-2 are enriched in presynaptic compartments of neurons, which contain mostly SVs and only very few LDCVs (Sadakata

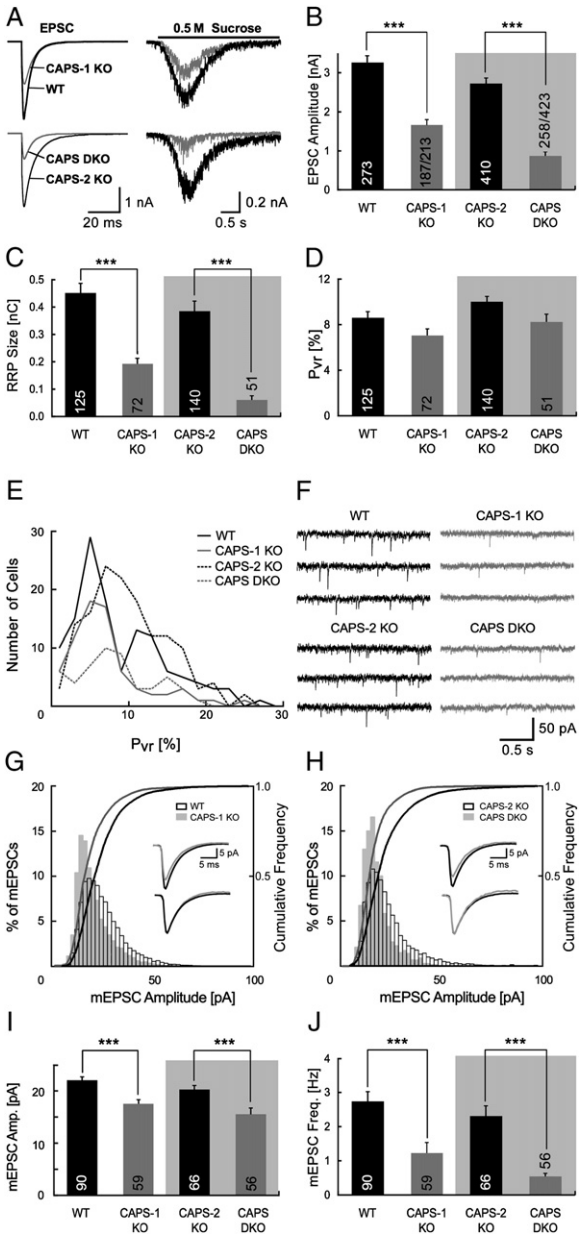

Figure 1. Reduced Glutamate Release and RRP Size in CAPS-1 KO and CAPS DKO Neurons

(A) EPSCs traces (left panel) and release induced by the application of 0.5 M sucrose solution for 6 s (right panel).

(B) Mean EPSC amplitudes measured in WT and CAPS-1 KO cells and in CAPS-2 KO and CAPS DKO cells (gray box), respectively.

(C) Mean RRP sizes as estimated by the charge integral measured after release induced by application of 0.5 M sucrose solution.

(D) Calculated mean P_{vr} (calculated by dividing the charge transfer during a single EPSC by the charge transfer measured during RRP release).

(E) Distribution of P_{vr} values shown in (D) (calculated by dividing the charge transfer during a single EPSC by the charge transfer measured during RRP release).

(F) mEPSC activity recorded at a holding potential of −70 mV.

(G) mEPSC amplitude distribution of WT and CAPS-1 KO neurons. The inset shows the averaged absolute (top) and normalized (bottom) mEPSC traces (n = 59–90).

et al., 2006; Speese et al., 2007; Speidel et al., 2003). The latter observation raises the question as to whether CAPS proteins may also have a function in SV exocytosis.

RESULTS

Defective SV Priming and Transmitter Release in the Absence of CAPS

We examined CAPS function in SV exocytosis by studying glutamatergic synaptic transmission in individual hippocampal neurons in autaptic culture (Bekkers and Stevens, 1991) taken from wild-type (WT), CAPS-1 KO (Stevens et al., 2005), CAPS-2 KO (Figure S1 in the Supplemental Data available with this article online), and CAPS-1/CAPS-2 double KO mice (CAPS DKO). We detected no morphological or functional differences between WT, heterozygous CAPS-2 KO, and homozygous CAPS-2 KO neurons in our analyses (data not shown), and therefore used CAPS-2 KO cells as controls in experiments with CAPS DKO neurons. Evoked excitatory postsynaptic current (EPSCs) amplitudes in CAPS-1 KO neurons were reduced to about 51% of WT values (Figures 1A and 1B, and Table 1), and 12% of all measured CAPS-1 KO cells showed no detectable EPSCs at all. This EPSC reduction was due to a parallel reduction in the size of the pool of fusion-competent and primed - or readily releasable - SVs (RRP), whose release can be triggered by the application of a hypertonic buffer containing 0.5 M sucrose (Rosenmund and Stevens, 1996; Stevens and Tsujimoto, 1995). CAPS-1 KO neurons showed a drastic reduction in RRP size to 42% of WT levels (Figure 1C and Table 1). The CAPS-1 KO cells that showed no detectable evoked EPSCs also failed to release transmitter in response to hypertonic buffer. The vesicular release probability P_{vr}, which we calculated by dividing the charge transfer during a single EPSC by the charge transfer measured during RRP release, was not different between WT and CAPS-1 KO neurons (Figure 1D and Table 1). In a total of 39% (165/423) of CAPS DKO neurons we were unable to elicit EPSCs or transmitter release in response to stimulation with hypertonic buffer. EPSC amplitudes and RRP sizes in the remaining active neurons were reduced to 32% and 15% of control levels, respectively (Figures 1A–1C and Table 1), while the P_{vr} was not changed (Figure 1D and Table 1). A detailed analysis of P_{vr} data from all cells of all genotypes showed that irrespective of the genotype most cells exhibited P_{vr} values of 6%–8% (Figure 1E), which indicates that the SV pools released in

(H) mEPSC amplitude distribution of CAPS-2 KO and CAPS DKO neurons. The inset shows the averaged absolute (top) and normalized (bottom) mEPSC traces (n = 56–66).

(I) Mean mEPSC amplitudes.

(J) Mean mEPSC frequencies.

Numbers in or above bars indicate the number of cells. Numbers in/over gray bars in (B) indicate cells with measurable EPSCs per total numer of cells measured. Stars above two bars indicate a statistically significant difference. Error bars indicate standard error of the mean (SEM).

Table 1. Synaptic Transmission in CAPS-1 KO and CAPS DKO Neurons

	WT	CAPS-1 KO	CAPS-2 KO	CAPS DKO
EPSC amplitude	3.3 ± 0.2 nA, n = 273	1.7 ± 0.1 nA, n = 187/213	2.7 ± 0.1 nA, n = 410	0.9 ± 0.1 nA, n = 258/423
RRP size	0.45 ± 0.04 nC, n = 125	0.19 ± 0.02 nC, n = 72	0.39 ± 0.04 nC, n = 140	0.06 ± 0.02 nC, n = 51
Vesicular release probability (P_{vr})	8.61% ± 0.04%, n = 125	7.1% ± 0.6%, n = 72	9.9% ± 0.4%, n = 140	8.3% ± 0.7%, n = 51
mEPSC amplitude	22.1 ± 0.6 pA, n = 90	17.5 ± 0.8 pA, n = 59	20.3 ± 0.8 pA, n = 66	15 ± 1 pA, n = 56
mEPSC frequency	2.7 ± 0.3 Hz, n = 90	1.2 ± 0.3 Hz, n = 59	2.3 ± 0.3 Hz, n = 66	0.54 ± 0.09 Hz, n = 56
mEPSC rise time	0.86 ± 0.02 ms, n = 90	0.99 ± 0.04 ms, n = 90	0.87 ± 0.05 ms, n = 66	0.98 ± 0.3 ms, n = 56
mEPSC decay time	3.83 ± 0.07 ms, n = 90	3.9 ± 0.1 ms, n = 90	3.98 ± 0.08 ms, n = 66	4.1 ± 0.1 ms, n = 56
EPSC amplitude, recalculated with reduced quantal amplitude		2.1 ± 0.2 nA, n = 187/213		1.1 ± 0.1 nA, n = 258/423
RRP size, recalculated with reduced quantal amplitude		0.24 ± 0.03 nC, n = 72		0.08 ± 0.02 nC, n = 51
EPSC amplitude in absence of PDBU	2.2 ± 0.3 nA, n = 20	0.8 ± 0.23 nA, n = 19	2.5 ± 0.43 nA, n = 21	0.4 ± 0.13 nA, n = 23
EPSC amplitude in the presence of 1 μM PDBU	3.6 ± 0.13 nA, n = 20	2.1 ± 0.4 nA, n = 19	4.0 ± 0.53 nA, n = 21	2.3 ± 0.33 nA, n = 23
EPSC potentiation ratio induced by 1 μM PDBU	1.8 ± 0.1, n = 20	3.4 ± 0.3, n = 19	1.8 ± 0.1, n = 21	10 ± 2, n = 23
Current amplitude 3 μM GABA	2.7 ± 0.1 nA, n = 120	2.3 ± 0.2 nA, n = 74	2.4 ± 0.2 nA, n = 61	2.1 ± 0.2 nA, n = 51
Current amplitude 10 μM KA	0.27 ± 0.01 nA, n = 113	0.22 ± 0.02 nA, n = 64	0.22 ± 0.02 nA, n = 60	0.33 ± 0.07 nA, n = 46
Current amplitude 300 μM KA			8 ± 1 nA, n = 10	8 ± 1 nA, n = 11
Current amplitude 100 μM Glu	2.0 ± 0.3 nA, n = 16	1.7 ± 0.2 nA, n = 14	2.4 ± 0.3 nA, n = 18	2.1 ± 0.3 nA, n = 19
Total number of synapses	871 ± 137, n = 23	717 ± 158, n = 16	720 ± 75, n = 33	759 ± 164, n = 26
Fraction of active synapses	55% ± 5%, n = 23	61% ± 5%, n = 16	45% ± 3%, n = 33	49% ± 3%, n = 26
Normalized Munc13-1 expression level (E18-E19 brain)	1.75 ± 0.09, n = 3	1.8 ± 0.1, n = 3	1.5 ± 0.1, n = 3	1.6 ± 0.3, n = 3
Normalized bMunc13-2 expression level	0.89 ± 0.05, n = 3	0.86 ± 0.05, n = 3	0.6 ± 0.2, n = 3	0.31 ± 0.05, n = 3
Percentage of Munc 13-1 positive Synaptobrevin-2 puncta			89% ± 2%, n = 6	87% ± 3%, n = 6
Fluorescence intensity Munc 13-1 in Synaptobrevin-2 positive puncta			75 ± 8, n = 6	68 ± 8, n = 6

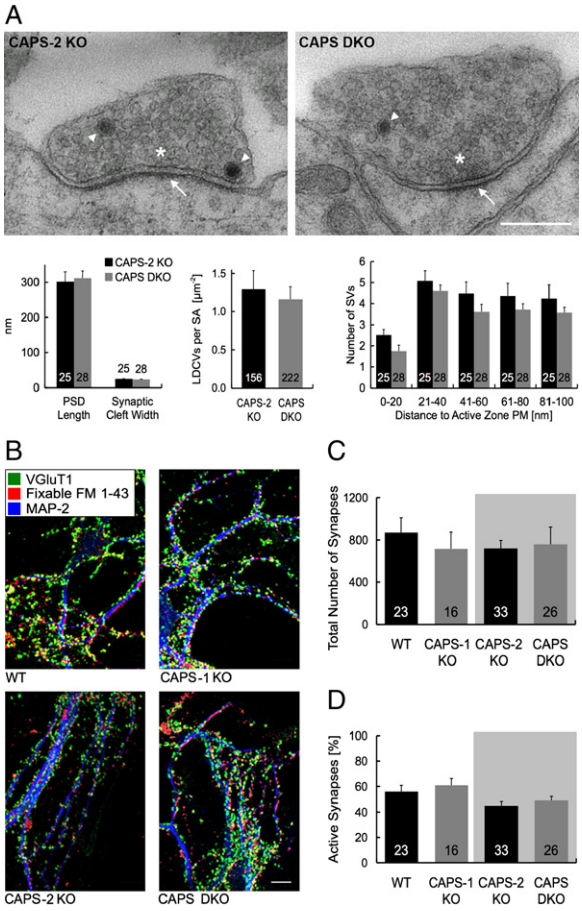

Figure 2. Synapse Morphology and Synapse Density in CAPS DKO Neurons

(A) Ultrastructural analysis of CAPS-2 and CAPS DKO neurons. The top panel shows example images of synapses from cells of the indicated genotype. Arrows indicate the postsynaptic density with the synaptic cleft, arrowheads indicate LDCVs, and a star indicates the SV cluster. Scale bar, 250 nm. The bottom panel shows from left to right the analysis of the basic synapse properties, the density of LDCVs, and the subsynaptic distribution of SVs. The distribution of SVs was measured using the orthogonal distance from the center of SVs to the plasma membrane opposite of the PSD (i.e., values for the 0–20 nm bin represent morphologically docked SVs). Numbers in or above the bars indicate the numbers of synapses. PM, plasma membrane; PSD, postsynaptic density; SA, synapse area.

(B) Examples of the fluorescence staining of autaptic neurons (red, fixable FM1-43; green, VGluT1; blue, MAP-2). Scale bar, 10 µm.

(C) Average total number of synapses in neurons determined by the VGluT1-positive puncta. Numbers in the bars indicate the numbers of cells.

(D) Average percentage of active synapses in neurons determined by the ratio of VGluT1/FM1-43 double-positive puncta *versus* all VGluT1-positive puncta. Numbers in the bars indicate the numbers of cells.

Error bars indicate standard error of the mean (SEM).

the presence and absence of CAPS proteins have similar release characteristics.

To test whether the secretory deficits in CAPS-1 KO and CAPS DKO neurons are caused by aberrant SV filling and concomitantly reduced quantal size, we analyzed miniature EPSCs (mEPSC). mEPSC amplitude and frequency in CAPS-1 KO neurons were reduced to 79% and 45% of control levels, respectively, while corresponding values for CAPS DKO cells were 77% and 23% of control levels, respectively (Figures 1F–1J and Table 1). Cumulative probability analyses of mEPSC amplitudes in CAPS-1 KO cells versus WT cells and in CAPS-DKO cells versus control cells revealed a uniform shift toward smaller mEPSC amplitudes in CAPS-1 KO and CAPS DKO neurons, while the kinetic characteristics of mEPSCs (i.e., rise and decay time constants) remained unaffected (Figures 1G and 1H, and Table 1). The uniform shift in EPSC amplitudes, which is already evident for small amplitudes (<15 pA), and the fact that mEPSC kinetics remain unchanged in the absence of CAPS proteins indicate that there is no selective defect in the release of a certain (e.g., larger) class of SVs in CAPS-1 KO and CAPS DKO cells. Responses of neurons to exogenously applied kainate, glutamate, or GABA were very similar across all genotypes (Table 1). As cell surface glutamate receptors, and in particular AMPA-type receptors that mediate fast synaptic transmission, are strongly enriched in postsynaptic membranes (Palmer et al., 2005), this finding supports the notion that the reduced mEPSC amplitude seen in CAPS-1 KO and CAPS DKO neurons (Figures 1G–1I) is mainly due to slightly reduced SV transmitter content (Speidel et al., 2005) and not caused by severe postsynaptic defects. An additional argument in support of the notion that postsynaptic receptor sensitivity is unchanged in CAPS DKO cells is provided by the fact that absolute evoked EPSC amplitudes in CAPS DKO neurons reach control levels after high-frequency stimulation (Figure 3C). The fact that the reduction in mEPSC amplitudes is similar in CAPS-1 KO and CAPS DKO cells (Figure 1I) while the mEPSC frequency is much more severely reduced in CAPS DKO cells (Figure 1J) indicates that a presynaptic priming defect and not a deficiency in SV filling is the main cause for the defective synaptic transmission in CAPS-1 KO and CAPS DKO cells. Indeed, even when we corrected our evoked EPSC amplitude and RRP size data for the reduced mEPSC amplitudes measured in CAPS-1 KO and CAPS DKO cells, the corresponding values were still highly significantly reduced as compared to the respective control condition (Table 1).

Normal Synaptic Ultrastructure and Synapse Numbers in the Absence of CAPS

To examine whether the priming defect in CAPS deficient neurons is associated with altered synapse morphology, we analyzed the ultrastructure of CAPS-2 KO and CAPS DKO synapses. We did not detect any changes in the width of the synaptic cleft or in the length of the postsynaptic density in CAPS DKO neurons. The number of SVs was slightly but not significantly decreased in CAPS DKO synapses (Figure 2A), including the population of morphologically docked SVs (Figure 2A bottom right; bin covering 0–20 nm distance of SV center to plasma

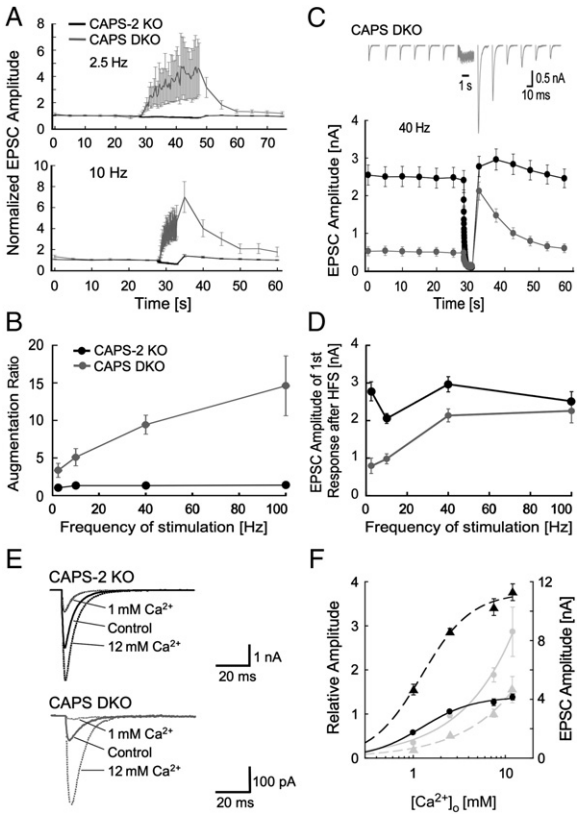

Figure 3. Short-Term Plasticity and Ca^{2+}-Dependence of Synaptic Transmission in CAPS-1 KO and CAPS DKO Neurons

(A) Change of synaptic strength during and following high-frequency stimulation. During a period of 0.2 Hz stimulation either a 2.5 Hz train (top) or a 10 Hz train (bottom) was applied (50 stimuli). The interval between the low- and high-frequency stimulation periods was 2 s. Data are normalized to the average EPSC amplitude of the first six data points obtained at 0.2 Hz stimulation (n = 28–70).

(B) Augmentation ratio after high-frequency stimulation from 2.5 Hz to 100 Hz (n = 21–196).

(C) Changes in absolute EPSC amplitudes induced by 40 Hz stimulation. The interval between the low- and high-frequency stimulation periods was 2 s. (n = 41–61). A sample trace from a CAPS DKO cell is shown above the summary data.

(D) Mean absolute augmented EPSC amplitudes after high-frequency stimulation from 2.5 Hz to 100 Hz (n = 21–196).

(E) EPSC traces triggered during the application of various external Ca^{2+} concentrations [see (F)] and the respective control (4 mM Ca^{2+}/4 mM Mg^{2+}).

(F) Apparent Ca^{2+} sensitivity of triggered release in CAPS-2 KO (black) and CAPS-DKO (gray) cells. Absolute (triangles) and relative (circles) EPSC amplitudes compared to the control condition are plotted as a function of the external Ca^{2+} concentration (1 to 12 mM Ca^{2+}, each with 1 mM Mg^{2+}; n = 12–15).

Error bars indicate standard error of the mean (SEM).

membrane). The density of LDCVs, which is very low in synapses of cultured hippocampal neurons, was similar in all genotypes tested (Figure 2A). These data indicate that the secretion deficit in CAPS DKO neurons is not caused by a major alteration of synapse morphology.

In addition, we determined the total number of synapses and the number of activatable synapses in autaptic neurons from the different CAPS genotypes by combining stainings with an antibody to the presynaptic marker VGluT1 and fixable FM1-43. During FM1-43 loading, synapses were stimulated with 86 mM K^+ (10 s), which causes long lasting an large increases in $[Ca^{2+}]_i$. We found that neither the total number of synapses nor the number of synapses activatable by a 10 s treatment in the presence of 86 mM K^+ were altered in CAPS-1 KO or CAPS DKO neurons (Figures 2B–2D). Thus, the reduced EPSC amplitudes measured in CAPS-1 KO and CAPS DKO neurons (Figures 1A and 1B) are likely caused by functional changes in presynaptic processes that are not detectable after massive stimulation in the prolonged presence of 86 mM K^+ (see also additional data below) and that do not directly affect the initial P_{vr} (Figures 1D and 1E).

Increases in $[Ca^{2+}]_i$ Can Transiently Bypass the Priming Defect Caused by CAPS Deletion

We next studied additional presynaptic transmitter release characteristics and short-term plasticity in CAPS DKO neurons, using CAPS-2 KO cells as controls. As in WT neurons, EPSC amplitudes in CAPS-2 KO neurons depressed progressively during 2.5 Hz (50 stimuli) and 10 Hz (50 stimuli) stimulation trains to reach 80% and 60% of the pre-train amplitudes (Figure 3A and Table 2). In contrast, EPSC amplitudes in CAPS DKO cells increased 5-fold over baseline values during 2.5 Hz and 10 Hz stimulation (Figure 3A and Table 2). The paired pulse depression ratios at these stimulation frequencies were identical between CAPS DKO and CAPS-2 KO neurons (Table 2), indicating that the frequency facilitation observed in CAPS DKO neurons is not due to changes in the initial release probability. Upon return from 10 Hz stimulation to low stimulation frequency, EPSC amplitudes were augmented up to 6-fold over baseline (Figures 3A and 3B, and Table 2). This post-train augmentation was more pronounced after 100 stimuli given at 40 Hz (10-fold) or 100 Hz (15-fold) (Figure 3B) such that augmented absolute EPSC amplitudes reached control values (Figures 3C and 3D, and Table 2). These data show that high-frequency stimulation triggers a process that turns poorly secreting CAPS DKO neurons transiently into neurons that can release transmitter at WT levels. This facilitation and augmentation effect is profound as early as 0.5–1 s and reaches WT levels 3 s after onset of high-frequency stimulation. As intervals of 0.5–3 s are too short for the complete glutamate loading of SVs, which takes several minutes in vitro (Maycox et al., 1988) and is estimated to take some 20 s in vivo (Takamori et al., 2006), these data argue strongly against the possibility that the deficit in transmitter release seen in CAPS DKO neurons (Figure 1) is mainly due to an SV loading defect. Rather, SVs seem to be loaded but require an additional boost provided by the high-frequency stimulation in order to become release-competent.

Table 2. Short-Term Synaptic Plasticity in CAPS DKO Neurons

	CAPS-2 KO	CAPS DKO
Facilitation ratio during 2.5 Hz stimulation	0.85 ± 0.03, n = 70	5 ± 2, n = 28
Facilitation ratio during 10 Hz stimulation	0.59 ± 0.03, n = 70	5 ± 2, n = 48
Augmentation ratio after 2.5 Hz stimulation	1.0 ± 0.3, n = 66	3 ± 1, n = 25
Augmentation ratio after 10 Hz stimulation	1.31 ± 0.07, n = 192	6 ± 1, n = 55
Augmentation ratio after 40 Hz stimulation	1.3 ± 0.1, n = 105	9 ± 1, n = 67
Augmentation ratio after 100 Hz stimulation	1.4 ± 0.1, n = 62	15 ± 4, n = 21
Paired pulse ratio (P_2/P_1) 10 ms interpulse interval	0.38 ± 0.03, n = 50	0.9 ± 0.3, n = 15
Paired pulse ratio (P_2/P_1) 25 ms interpulse interval	0.83 ± 0.03, n = 95	1.2 ± 0.3, n = 79
Paired pulse ratio (P_2/P_1) 100 ms interpulse interval	0.90 ± 0.02, n = 196	0.95 ± 0.04, n = 66
Paired pulse ratio (P_2/P_1) 400 ms interpulse interval	0.93 ± 0.02, n = 64	1.1 ± 0.2, n = 27
mEPSC amplitude at resting condition	22 ± 1 pA, n = 7	18.5 ± 0.9 nA, n = 7
mEPSC amplitude after 40 Hz stimulation	25 ± 1 pA, n = 7	21 ± 1 nA, n = 7
mEPSC frequency at resting condition	39 ± 10 Hz, n = 7	4.0 ± 0.7 Hz, n = 7
mEPSC frequency after 40 Hz stimulation	127 ± 19 Hz, n = 7	29 ± 8 Hz, n = 7
EPSC amplitude 1 mM Ca^{2+}/1 mM Mg^{2+}	4.7 ± 0.4 nA, n = 15	0.62 ± 0.06 nA, n = 12
EPSC amplitude 2.5 mM Ca^{2+}/1 mM Mg^{2+}	8.6 ± 0.2 nA, n = 15	1.7 ± 0.1 nA, n = 12
EPSC amplitude 7.5 mM Ca^{2+}/1 mM Mg^{2+}	10.3 ± 0.6 nA, n = 15	3.3 ± 0.3 nA, n = 12
EPSC amplitude 12 mM Ca^{2+}/1 mM Mg^{2+}	11.3 ± 0.6 nA, n = 15	5 ± 1 nA, n = 12
Relative EPSC amplitude 1 mM Ca^{2+}/1 mM Mg^{2+}	0.57 ± 0.04, n = 15	0.36 ± 0.04, n = 12
Relative EPSC amplitude 2.5 mM Ca^{2+}/1 mM Mg^{2+}	1.06 ± 0.03, n = 15	0.97 ± 0.06, n = 12
Relative EPSC amplitude 7.5 mM Ca^{2+}/1 mM Mg^{2+}	1.26 ± 0.07, n = 15	1.9 ± 0.2, n = 12
Relative EPSC amplitude 12 mM Ca^{2+}/1 mM Mg^{2+}	1.39 ± 0.07, n = 15	2.9 ± 0.6, n = 12
Relative RRP size after 10Hz stimulation	0.56 ± 0.04, n = 20	2.8 ± 0.4, n = 16
Relative RRP size after 40Hz stimulation	0.64 ± 0.05, n = 25	6 ± 1, n = 26
Time constant of onset of tonic release during 40 Hz Stimulation	τ = 0.18 s, n = 68	τ = 0.21 s, n = 64
Initial EPSC amplitude of cells used for calcimycin experiments	3.1 ± 0.5, n = 31	0.5 ± 0.2, n = 25/29
Total charge induced by 10 μM calcimycin	4.5 ± 0.8 nC, n = 31	6 ± 1 nC, n = 29
Amplitude of NMDA component relative to AMPA component	0.13 ± 0.02, n = 9	0.11 ± 0.01, n = 8
Time constants of decay of the relative NMDA component during application of 3 μM MK-801	τ_f = 29 ± 4 s, 80%, τ_s = 382 ± 112 s, 20%	τ_f = 34 ± 5 s, 59%, τ_s = 320 ± 73 s, 41%

The transient amelioration of the transmission defect in CAPS DKO neurons after high-frequency stimulation could be a result of the increase in $[Ca^{2+}]_i$ during and after high-frequency stimulation. We therefore examined the Ca^{2+}-sensitivity of evoked release from CAPS DKO neurons by measuring EPSC amplitudes as a function of the external Ca^{2+} concentration $[Ca^{2+}]_o$. For the analysis, EPSC values obtained with 1, 2.5, 7.5, and 12 mM $[Ca^{2+}]_o$, each in the presence of 1 mM $[Mg^{2+}]_o$, were normalized to values obtained under control conditions (4 mM $[Ca^{2+}]_o$/4 mM $[Mg^{2+}]_o$). CAPS DKO neurons showed stronger potentiation of EPSC amplitudes at 12 mM $[Ca^{2+}]_o$ than control cells. The corresponding normalized $[Ca^{2+}]_o$ dose-response curves for control and CAPS DKO neurons were similar at extracellular Ca^{2+} concentrations of up to 2–3 mM and then diverged (Figures 3E and 3F, and Table 2). The normalized and absolute $[Ca^{2+}]_o$ dose-response curve for CAPS DKO cells did not saturate within the $[Ca^{2+}]_o$ concentration range tested (Figure 3F), most likely because of a Ca^{2+} dependent increase in SV priming in the CAPS DKO cells (see below). These data and additional findings reported below indicate that the Ca^{2+} dependent triggering step of exocytosis is essentially unaffected in CAPS DKO cells. However, a minor effect of

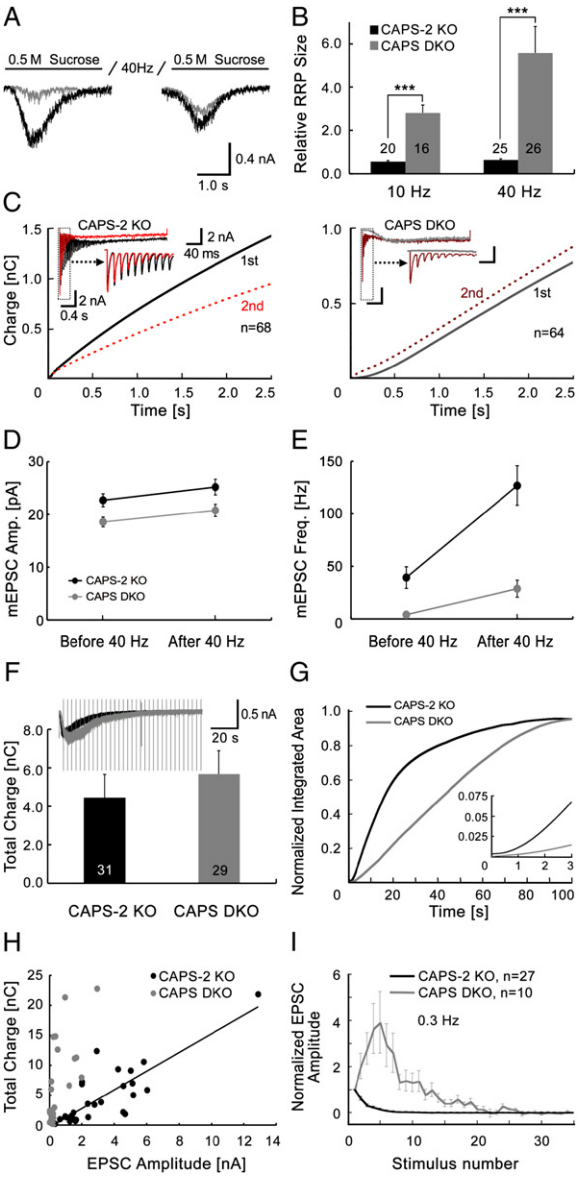

Figure 4. Ca^{2+}-Dependent Transient Recovery of RRP and EPSC Amplitudes in CAPS DKO Neurons

(A) Release induced by application of 0.5 M sucrose solution for 6 s before and after 40 Hz stimulation, recorded from a CAPS-2 KO (black) and a CAPS DKO neuron (gray).

(B) Average ratios of the RRP sizes (after *versus* before 40 Hz train).

(C) Average time course of the charge transfer induced by double 40 Hz stimulations separated by a 2 s break. Insets show example traces recorded during the double 40 Hz stimulation (first train, black or gray; second train red or crimson).

(D) mEPSC amplitude before and 2–12 s after 40 Hz stimulation (n = 7).

(E) mEPSC frequency before and 2–12 s after 40 Hz stimulation (n = 7).

(F) Total charge transfer induced by the application of calcimycin for 100 s. The inset shows representative raw traces (CAPS-2 KO, black trace; CAPS DKO, gray trace). Vertical lines at 3 s intervals represent stimulation artifacts resulting from intermittent monitoring of evoked EPSCs.

(G) Time course of the charge transfer induced by the application of calcimycin, normalized to the last data point. The inset shows a magnification of the first three seconds.

(H) Total charge transfer induced by calcimycin, recorded from individual cells plotted against initial evoked EPSCs from the same cells. The slope of the fit for the data from CAPS-2 KO neurons is 1.56 (black line). Data from CAPS DKO neurons did not show any correlation between calcimycin induced charge transfer and initial EPSC amplitude.

(I) Mean amplitudes of evoked EPSCs (stimulated at 0.3 Hz) recorded during the application of calcimycin, normalized to the first data point.

Numbers in or above bars indicate the numbers of cells. Stars above two bars indicate a statistically significant difference. Error bars indicate standard error of the mean (SEM).

the CAPS deficiency on the triggering step cannot be formally excluded on the basis of the present data. We also determined RRP sizes at 7.5 mM $[Ca^{2+}]_o$/1 mM $[Mg^{2+}]_o$ and at 12 mM $[Ca^{2+}]_o$/1 mM $[Mg^{2+}]_o$, and calculated the corresponding P_{vr} values, which were similar (~11%) in CAPS DKO and control cells. This finding further supports our conclusion that the Ca^{2+} dependent triggering step of exocytosis is operating normally in CAPS DKO neurons.

To examine whether the augmentation induced by high-frequency stimulation in CAPS DKO neurons is caused by an increase in the RRP, we compared RRP measurements before and 2 s after 10 Hz or 40 Hz stimulation trains (50 and 100 stimuli, respectively). In control cells, 10 Hz and 40 Hz stimulation reduced the RRP size to 56% and 64% of the pre-train value, respectively, consistent with the notion that synaptic depression during high-frequency stimulation is caused mainly by RRP depletion (Otsu and Murphy, 2004; Zucker and Regehr, 2002). In CAPS DKO neurons, the RRP size after 10 Hz and 40 Hz stimulation increased 2.8-fold and 5.6-fold, respectively (Figures 4A and 4B, and Table 2). Thus, an increase in the RRP size is the main reason for the pronounced facilitation and augmentation that is induced by high-frequency stimulation trains in CAPS DKO neurons.

To test how this newly formed RRP induced by high-frequency stimulation in CAPS DKO neurons contributes to transmitter release, we studied responses to two 40 Hz action potential trains (100 stimuli) spaced at a 2 s interval. In control neurons, phasic EPSCs in response to the second 40 Hz train depressed much more rapidly than responses to the first train, which resulted in an overall reduction of combined phasic and tonic release during the second train (Figure 4C, left). However, in CAPS DKO neurons the first train mainly evoked tonic release, as seen by the downward shift of the baseline (Figure 4C, right), while the second train evoked strong but rapidly depressing phasic EPSCs on the background of unaltered tonic release (Figure 4C, right). As a consequence, the total release in CAPS DKO neurons during the second train was slightly higher than during the first train (Figure 4C, right). Interestingly, the phasic EPSCs induced in CAPS DKO neurons after the first high-frequency train always decayed within 6–7 stimuli, irrespective of the stimulation frequency used (data not shown). Also, the amount of tonic release during the first and second train was similar in CAPS DKO neurons (Figure 4C, right), which supports the notion that there is no major SV filling deficit in the CAPS DKO neurons that would be ameliorated by the

high-frequency stimulation. In an additional set of experiments, we found that along with the RRP size and evoked EPSCs, the mEPSC frequency increased 7.3-fold in CAPS DKO neurons immediately following high-frequency stimulation, approaching the levels observed in control cells before high-frequency stimulation (Figure 4E and Table 2). Under the same conditions, we found mEPSC amplitudes to also be slightly increased in both control and CAPS DKO cells (Figure 4D and Table 2). This apparent increase in mEPSC amplitudes in CAPS DKO and control neurons is most likely due to detection problems and simultaneous sampling of multiple mEPSCs at the high mEPSC frequencies measured here, and therefore not physiologically relevant.

Given that the facilitation, augmentation, and RRP increase in CAPS DKO cells upon high-frequency stimulation (Figures 3 and 4) are likely caused by transient increases of $[Ca^{2+}]_i$, we next investigated synaptic activity in CAPS DKO neurons while clamping $[Ca^{2+}]_i$ at high levels. We monitored spontaneous and evoked release in the presence of the Ca^{2+} ionophore calcimycin (10 μM). This caused a massive increase of spontaneous glutamate release that was quantitatively similar in control and CAPS DKO neurons, including cells that did not exhibit any evoked EPSCs (Figures 4F and 4G). The latter observation indicates that responding and non-responding CAPS DKO neurons represent only quantitatively different variants of the same mutant phenotype. Total calcimycin-induced release was proportional to the initial EPSC amplitude in CAPS-2 KO neurons but not in CAPS DKO cells (Figure 4H). Thus, the $[Ca^{2+}]_i$-increase induced by calcimycin enforces the release of the same number of SVs in both genotypes, irrespective of the initial release capacity. Despite this similarity in the extent of calcimycin-induced release between control and CAPS DKO neurons (Figure 4F), the time courses of the release were different. Control cells started to release immediately after application of calcimycin while the onset of release after calcimycin application was delayed and slower in CAPS DKO neurons (Figures 4F and 4G). Also, phasic EPSCs measured at 0.3 Hz throughout calcimycin treatment were different in the two genotypes tested. EPSCs in control neurons depressed rapidly, while EPSCs in CAPS DKO cells facilitated transiently and then depressed gradually (Figure 4I). Fura-2 measurements showed that the time courses and amplitudes of $[Ca^{2+}]_i$ changes induced by high-frequency stimulation and calcimycin application are very similar in neurites of control and CAPS DKO cells (Figure S2), indicating that Ca^{2+} handling is normal in the absence of CAPS. P_{vr} values at high Ca^{2+}-concentrations were similar in control and CAPS DKO cells (see above). Thus, the delayed spontaneous (Figures 4F and 4G) and transiently increased evoked release (Figure 4I) in CAPS DKO neurons upon calcimycin addition is likely due to the fact that SVs in mutant cells require elevated $[Ca^{2+}]_i$ for 0.5–2 s in order to be primed and recruited for Ca^{2+}-induced release.

We next examined whether the new $[Ca^{2+}]_i$-induced fusion competent SVs in CAPS DKO neurons originate from previously silent synapses or from increased priming in already active synapses, or both. To address this question, we monitored the NMDA components of EPSCs elicited at 0.3 Hz in the presence of the irreversible NMDA receptor open-channel blocker MK-801, before and after a 40 Hz stimulation train, during which no MK-801 was present (Figures 5A and 5B) (Rosenmund et al., 1993). At the onset of the experiment, NMDA/AMPA ratios of EPSCs were similar in CAPS DKO and control cells (Figure 5B, inset). EPSCs were stimulated in the presence of 10 μM glycine, 2.7 mM Ca^{2+} (no Mg^{2+}), and the progressive block of NMDA-mediated EPSCs by MK-801 was analyzed. In CAPS-2 KO control neurons, the MK-801 block exhibited decay kinetics with a rapid and a slow component during 100 stimuli at 0.3 Hz (Table 2). Following an intermittent 40 Hz stimulation (100 stimuli) in the absence of MK-801, no new NMDA component was detectable upon return to 0.3 Hz stimulation. This indicates that all active synapses had been blocked during the first MK-801 treatment (Figures 5A and 5B). In responding CAPS DKO neurons, NMDA-mediated EPSCs decayed with a delay (Figures 5A and 5B, and Table 2). This delay was due to the fact that the NMDA component was increased during the first five stimuli (Figure 5B), most likely because even the 0.3 Hz stimulation causes a $[Ca^{2+}]_i$-increase that suffices to partially bypass the CAPS requirement, prime SVs, and boost synaptic release. Strikingly, a new NMDA-mediated EPSC component appeared after the intermittent 40 Hz stimulation but decayed very rapidly. The first EPSC measured 2 s after the 40 Hz stimulation train had a dramatically increased NMDA component compared to the response before the stimulation train, approaching the values seen before MK-801 treatment (Figures 5A and 5B). Even non-responding cells that did not release at all during the first phase of 0.3 Hz stimulation in the presence of MK-801 showed a new NMDA-mediated EPSC component after the intermittent 40 Hz stimulation (~0.09 relative to the AMPA amplitude, data not shown). Similar data were obtained when 300 instead of 100 stimuli at 40 Hz were applied, and no new NMDA component was detectable when the 40 Hz train was given in the presence of MK-801 (data not shown). Together, these results indicate that in CAPS DKO neurons the facilitation and augmentation upon high-frequency stimulation are to a large extent due to the Ca^{2+}-dependent 'awakening' of previously inactive or very weakly active synapses. That most synapses in CAPS DKO neurons can be activated if the stimulation and concomitant increase in $[Ca^{2+}]_i$ is sufficiently robust is nicely illustrated by the FM1-43 loading data (Figures 2B and 2D).

Munc13s and CAPS are Essential Components of the Same Priming Pathway

Munc13-1 KOs (Augustin et al., 1999; Rosenmund et al., 2002) are the only other known mouse mutants with a priming deficit that is similar in type and extent to the one seen in CAPS-1 KOs and CAPS DKOs. Like CAPS-1 KO and CAPS DKO neurons, Munc13-1 deficient

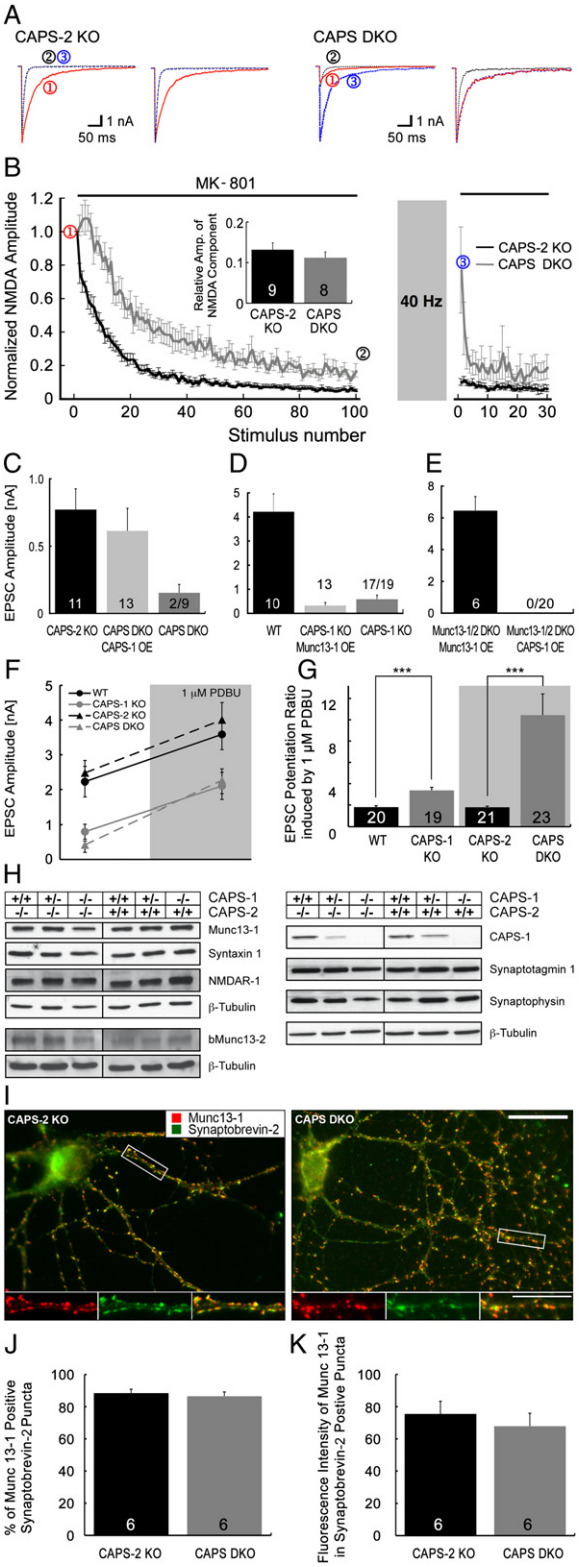

Figure 5. Awakening of Silent Synapses in CAPS DKO Neurons, and Munc13-1 Expression and Localization in CAPS Deficient Neurons

glutamatergic hippocampal neurons, in which only Munc13-2 is still present, show strong Ca^{2+} dependent augmentation after high-frequency stimulation (Rosenmund et al., 2002). This augmentation in Munc13-1 KO neurons is due to parallel increases in RRP size and P_{vr} (Rosenmund et al., 2002), while in the CAPS DKO cells, the augmentation after high-frequency stimulation is mainly due to a change in RRP size.

In view of the similarity between Munc13-1 KO and CAPS-1 KO or CAPS DKO cells, it is possible that Munc13 proteins and CAPS proteins operate in the same priming process and that the residual, strongly Ca^{2+} dependent transmitter release activity in CAPS-1 KO and CAPS DKO cells is due to Munc13 dependent SV priming. To test these possibilities, we performed two types of experiments. In a first set of experiments, we examined whether the priming deficit of CAPS deficient and Munc13-1/2 DKO cells can be rescued by overexpression of Munc13-1 or CAPS-1, respectively. We found that overexpression of Munc13-1 in CAPS-1 KO cells and of CAPS-1 in Munc13-1/2 DKO cells failed to cross-rescue the mutant phenotypes (Figures 5D and 5E) while overexpression of CAPS-1 rescued the CAPS

(A, B) Synaptic NMDA EPSCs were blocked by eliciting a series of 100 EPSCs at 0.3 Hz in the presence of MK-801 (5 μM). Cells were then stimulated at 40 Hz for 2.5 s in the absence of MK-801 followed by 30 EPSCs at 0.3 Hz again in the presence of MK-801.

(A) EPSCs at the beginning of the first application of MK-801 (1), at the end of the first application of MK-801 (2), and at the beginning of the second application of MK-801 (3) (example neurons). The left panels show the absolute EPSCs, the right panels show the same example traces normalized to the AMPA component.

(B) Averaged normalized NMDA-mediated amplitudes plotted against the stimulus number during the first application of MK-801 and during the second application of MK-801 (n = 8–9). The inset shows the mean NMDA component relative to the AMPA component.

(C–E) Mean EPSC amplitudes measured in cells with the indicated genotype and after Semliki Forest Virus mediated overexpression of the indicated proteins. OE, overexpression.

(F) EPSC amplitudes in the absence and presence of 1 μM PDBU (n = 19–23).

(G) EPSC potentiation induced by 1 μM PDBU.

(H) Expression of synaptic proteins in cultured hippocampal neurons of mice with the indicated genotype. Cell homogenates (20 μg of protein per lane from DIV 14 neurons) were analyzed by Western blotting using antibodies against the indicated proteins. For the detection of the bMunc13-2 signal, 30 μg of protein from DIV 21 neurons were loaded onto each lane.

(I) Combined immunofluorescence detection of Synaptobrevin-2 (green) and Munc13-1 (red) in cultured hippocampal neurons, demonstrating that Munc13-1 is localized at presynaptic terminals in CAPS DKO neurons and CAPS-2 KO neurons. Insets show a magnification of the marked section (white box) in each neuron. Scale bars, 20 μm and 10 μm (inset).

(J) Mean percentage of Synaptobrevin-2 positive puncta colocalizing with Munc13-1 positive (100 synapses per cell).

(K) Fluorescence intensity of Munc13-1 in Synaptobrevin-2 positive puncta from (J).

Numbers in or above bars indicate the numbers of cells. Stars above two bars indicate a statistically significant difference. Error bars indicate standard error of the mean (SEM).

DKO phenotype (Figure 5C). These data indicate that CAPS proteins and Munc13 proteins are unlikely to operate in independent parallel priming pathways. Rather, the failure of our cross-rescue attempts is consistent with the possibility that the two priming factors operate in series in the same pathway or jointly as equally essential components of the same priming apparatus. In a second set of experiments, we tested whether the remaining, strongly Ca^{2+} dependent transmitter release activity in CAPS-1 KO and CAPS DKO cells is due to Munc13 dependent SV priming. For this purpose, we took advantage of the fact that in our assay system and under our assay conditions, phorbol ester dependent stimulation of transmitter release is absolutely dependent on Munc13 proteins (Rhee et al., 2002). We found that treatment with 1 μM of the phorbol ester PDBU caused robust increases of evoked EPSC amplitudes in all cells of all genotypes tested (Figure 5F and Table 1), including cells that failed to show evoked EPSCs before PDBU treatment (data not shown). Most notably, the PDBU-induced potentiation of evoked EPSCs was strongest in CAPS DKO cells (10-fold) in which absolute PDBU-potentiated EPSCs reached values measured in control cells before PDBU treatment (Figures 5F and 5G, and Table 1). These findings provide strong support of the notion that the remaining SV priming and release activity in CAPS DKO neurons is mediated by Munc13 proteins, most likely Munc13-1 and Munc13-2.

In order to determine whether the SV priming deficit in CAPS-1 KO and CAPS DKO neurons could be due to a loss of Munc13 proteins from synapses, we performed a quantitative analysis of Munc13 expression, focusing on Munc13-1 and bMunc13-2, which are the two main Munc13 isoforms expressed in mature neurons in culture and in situ. Western blot analyses of hippocampal cultures and E18-E19 brain homogenates showed that total Munc13-1 expression levels are similar in control and CAPS deficient neurons and brains (Figure 5H and Table 1).

In addition, quantitative immunostaining studies on cultured neurons using antibodies to Munc13-1 and Synaptobrevin-2 showed that the levels of Munc13-1 in synapses is unaltered in CAPS DKO neurons in culture, as determined by the proportion of Synaptobrevin-2-positive puncta containing Munc13-1 and by the fluorescence intensity of Munc13-1 immunofluorescence signals at Synaptobrevin-2-positive synapses (Figures 5I–5K and Table 1). Interestingly, we found the bMunc13-2 expression levels in cultured neurons and E18-19 brain homogenates from CAPS DKO brain to be reduced by 48% as compared to the control condition (Figure 5H and Table 1). While this expression decrease may be indicative of a functional interaction between bMunc13-2 and CAPS proteins, it is extremely unlikely to contribute to the CAPS DKO phenotype because heterozygous and even homozygous Munc13-2 KO neurons are functionally indistinguishable from WT cells (Varoqueaux et al., 2002). Taken together, our quantitative analysis of Munc13 expression in control and mutant neurons indicates that the SV priming deficit in CAPS-deficient neurons is not caused by altered Munc13 levels at synapses.

DISCUSSION

Our study shows that CAPS proteins are essential for the generation of readily releasable SVs. The severity of the priming deficit in CAPS DKO neurons is similar to that seen in mouse mutants with the most severe and specific priming defects known so far, i.e., Munc13-1 KOs (Augustin et al., 1999; Rosenmund et al., 2002) and Munc13-1/2 DKOs (Varoqueaux et al., 2002). This establishes CAPS proteins as novel essential components of the SV priming machinery that supports phasic Ca^{2+} triggered transmitter release.

Our rescue experiments show that the priming deficit in CAPS DKO neurons can be reverted by re-expression of CAPS-1 but not by overexpression of Munc13-1, and that SV priming in Munc13-1/2 DKO neurons remains blocked after overexpression of CAPS-1 (Figures 5C–5E). This indicates that the priming defect in CAPS DKO neurons reflects a cell autonomous phenotype, which is supported by the observation that the aberrant locomotor activity of *C. elegans unc-31* mutants can be rescued by specific re-expression of Unc-31 in motorneurons (Charlie et al., 2006). In addition, our analysis of Munc13 expression (Figure 5H and Table 1) and localization in CAPS DKO neurons (Figures 5I–5K) shows that the deficiency of the priming activity in CAPS DKO cells is not due to a loss of Munc13s from presynaptic terminals. This notion is supported by the fact that treatments causing increases of $[Ca^{2+}]_i$ can transiently activate SV priming and phasic Ca^{2+} triggered transmitter release from previously inactive or very weakly active synapses, possibly by stimulating Munc13s localized at the active zone (Figures 3 and 4). Indeed, treatment of CAPS-1 KO and CAPS DKO neurons with PDBU, which selectively activates a Munc13-dependent priming process in our preparation (Rhee et al., 2002), caused robust increases of evoked EPSC amplitudes (Figure 5F and Table 1), including cells that failed to show evoked EPSCs before PDBU treatment. This indicates that the remaining SV priming and release activity in CAPS deficient neurons is mediated by Munc13 proteins, most likely Munc13-1 and Munc13-2. Based on these findings, we propose a model of concerted Munc13/CAPS action. Either, the two proteins act in series, with Munc13s generating a primed pool of SVs that can support tonic release (Figure 4C) but that need to be stabilized in a rapidly releasable state by CAPS proteins in order to support evoked phasic release. Alternatively, CAPS and Munc13s act in concert as equally essential components of the SV priming apparatus. The molecular basis of this concerted Munc13/CAPS action remains unknown, but it is likely that the Munc13-homology domain 1 in CAPS proteins (Koch et al., 2000) is partially responsible for their priming function. This domain is part of the minimal priming domain in Munc13s and involved in Syntaxin binding (Basu et al., 2005; Stevens et al., 2005). Thus,

Munc13s and CAPS proteins may jointly determine SV priming by regulating Syntaxin function and SNARE complex formation.

Our data demonstrate for the first time a direct role of CAPS in SV fusion. For a number of reasons our observations in CAPS deficient neurons cannot be interpreted as an indirect effect of altered LDCV function (Speese et al., 2007; Tandon et al., 1998). First, the effects of LDCV-derived neuropeptides and neuromodulators on synaptic transmission in glutamatergic hippocampal neurons are of a subtle modulatory nature. A perturbation of such modulatory effects cannot explain the severe priming deficit seen in CAPS DKO cells (Figures 1A–1D). Indeed, mice lacking the peptide hormone convertases/peptidases PC1/3, PC2, or CPE are all viable and fertile, and do not exhibit any of the striking neurological characteristics seen in CAPS1 KOs and CAPS DKOs (i.e., total paralysis and perinatal lethality) (Beinfeld et al., 2005; Cawley et al., 2004; Furuta et al., 1997; Pan et al., 2006; Zhu et al., 2002). Based on the macroscopic phenotypes of mice lacking PC1/3, PC2, or CPE alone, it is extremely unlikely that the SV priming deficit seen in CAPS-deficient neurons is indirectly caused by aberrant LDCV-dependent peptide hormone release. Second, the astrocytes we used for autaptic cultures were from WT mice, excluding the possibility that interference with an LDCV-based paracrine regulatory effect by astrocytes causes the CAPS DKO phenotype. In addition, autocrine and neuronal paracrine effects are minimal in autaptic neuron cultures. Third, CAPS DKO neurons develop normally and generate morphologically normal synapses at normal numbers (Figure 2), and the priming deficiency in CAPS DKO neurons is reverted 12-14 h after re-expression of CAPS-1 (Figure 5C). It is therefore unlikely that a perturbation of an LDCV-based autocrine effect causes grossly abnormal cell differentiation resulting in the CAPS DKO phenotype. Fourth, the phenotype of CAPS DKO neurons is different from that seen in KO mice lacking proteins that are essential for LDCV biogenesis such as Chromogranin (Mahapatra et al., 2005). Finally, the phenotypes of neurons with severe perturbations in both SV and LDCV secretion such as SNAP-25 KO (Washbourne et al., 2002) or Synatobrevin 2 KO neurons (Schoch et al., 2001) are very different from the phenotype caused by CAPS deficiency. The observation that cultured neurons from *C. elegans unc-31* mutants exhibit normal FM4-64 dye loading is consistent with the possibility that Unc-31 is not involved in synaptic vesicle exocytosis (Speese et al., 2007). However, this conclusion is not justified because our own FM1-43 loading experiments (Figures 2B–2D) show that the massive stimulation used in such dye loading experiments, i.e., application of 80–90 mM K^+ for extended periods of time, overrides the CAPS dependence of synaptic vesicle priming, as do the application of calcimycin and other measures to profoundly increase $[Ca^{2+}]_i$ (Figures 3 and 4).

Interestingly, the severe RRP size defect seen in CAPS DKO neurons during low frequency stimulation is transiently reverted if these neurons are stimulated at high-frequency or if $[Ca^{2+}]_i$ is increased by other means (Figures 3 and 4). Neurons that were previously deficient in phasic action potential-triggered transmitter release and only showed tonic release (Figure 4C) start to show such phasic release after transient increases in $[Ca^{2+}]_i$ and a concomitant increase in SV priming and RRP sizes (Figures 3 and 4). It is unlikely that these $[Ca^{2+}]_i$-mediated effects are due to aberrant Ca^{2+}-handling in CAPS DKO neurons, because our Fura-2 imaging data indicate that $[Ca^{2+}]_i$-transients in neurites induced by calcimycin treatment or high-frequency stimulation are similar in control and CAPS DKO neurons (Figure S2), yet release characteristics are strikingly different. It is likely that this $[Ca^{2+}]_i$-dependent priming process is executed by essential priming protein of the Munc13 family, all of which are known to bind and be stimulated by Ca^{2+}/CaM (Dimova et al., 2006; Junge et al., 2004) and diacylglycerol or phorbol esters (Rhee et al., 2002). As mentioned above, this notion is supported by the fact that the priming deficit of CAPS-1 KO and CAPS DKO neurons can be reverted by phorbol ester application (Figures 5F and 5G).

Based on several lines of evidence, it is very unlikely that the remaining release in CAPS-1 KO and CAPS DKO neurons under resting conditions (Figure 1) and the augmented release in CAPS deficient neurons after rises in intracellular Ca^{2+} concentrations (Figures 3 and 4) originate from a distinct CAPS-specific pool of releasable SVs or synapses. For example, many CAPS-1 KO cells and almost half of the CAPS DKO cells we measured do not release transmitter at all if stimulated at low stimulation frequencies (Figure 1B). This finding indicates that in many neurons ultimately all releasable SVs at all synapses are affected by the CAPS deficiency. In addition, CAPS-deficient neurons and the respective control cells exhibit similar release probabilities at control (Figures 1D and 1E) and increased Ca^{2+} concentrations (~11% at 7.5 mM $[Ca^{2+}]_o$/1 mM $[Mg^{2+}]_o$ or 12 mM $[Ca^{2+}]_o$/1 mM $[Mg^{2+}]_o$), and mEPSC kinetics are similar in control and CAPS-1 KO or CAPS DKO neurons (Table 1). This indicates that SVs of similar type are released with similar characteristics at control and CAPS-deficient synapses. We therefore conclude that CAPS proteins are generally essential priming proteins in glutamatergic hippocampal neurons.

EXPERIMENTAL PROCEDURES

Mutant Mouse Strains

CAPS-1 KO mice were published previously (Speidel et al., 2005). CAPS-2 KO mice were generated by homologous recombination in embryonic stem cells (Figure S1). Details are provided in Supplemental Data.

Cell Culture and Electrophysiology

Microisland cultures of hippocampal neurons were prepared as described (Pyott and Rosenmund, 2002). Cells were whole-cell voltage clamped at −70 mV with an EPSC10 (HEKA) under control of the Patchmaster 2 program (HEKA). All analyses were performed using Axograph 4.1 (Axon Instruments) and MiniAnalysis (Synaptosoft). The RRP size was determined by a 6 s application of the external saline solution made hypertonic by the addition of 0.5 M sucrose. Recordings

of mEPSCs were performed in the presence of 300 nM tetrodotoxin (TTX). EPSCs were evoked by depolarizing the cell from −70 to 0 mV for 2 ms. The effect of high-frequency stimulation on the amplitude of EPSCs was measured by applying depolarisations at frequencies of 2.5, 10, 40, and 100 Hz for either 50 or 100 stimuli. Error bars indicate standard error. Statistical significance was tested using Student's t test.

Morphometry and Immunostaining

Hippocampal neurons were grown for 14–28 days and then stained at 30°C for 10 s with 20 μM fixable FM1-43 (Molecular Probes) in modified, depolarizing medium containing 86 mM K^+ and 83.5 mM Na^+, immediately followed by a 30 s incubation with the same dye concentration in standard medium. Cells were washed with medium, fixed for 5 min with 2.5% formaldehyde in medium and then incubated for 15 min with 5% formaldehyde in PBS. Reactive sites were blocked with 25 mM glycine in PBS for at least 30 min. Then cell membranes were permeabilized under mild conditions to avoid the formation of dispersive aggregates from membrane contents and the membrane staining dye. For this purpose, the cells were kept for 20 min in 1 mM sodium cholate (Sigma) in an otherwise salt free 300 mM sucrose solution. Before and after the permeabilization, cells were washed with 300 mM sucrose to remove salt and detergent residues. To identify all synapses independently of their exocytotic activity, cultures were stained with a primary monoclonal antibody directed against VGluT1 (Synaptic Systems) and a guinea pig antibody against MAP-2 (Chemicon), followed by Alexa-546- and Alexa-633-labeled secondary antibodies (Molecular Probes). Samples were used without mounting to record fluorescence images with an inverse staged Zeiss LSM 410 confocal microscope equipped with a 40x oil immersion objective and Zeiss LSM 3.98 software. Excitatory synapses were identified on the basis of the VGluT1 and FM1-43 stains, and were separately analyzed as total number of synapses (all VGluT1 positive puncta) and active synapses (VGluT1/FM1-43 colocalized puncta). Synapses were counted as described (Varoqueaux et al., 2002). For routine quantitative immunostaining, neurons were prepared from E18-E19 hippocampi, and cultured and processed as described (Varoqueaux et al., 2002). Error bars indicate standard error. Statistical significance was tested using Student's t test.

Electron Microscopy

For electron microscopy, hippocampal cultures were processed and analyzed as described (Varoqueaux et al., 2002). Details are provided in Supplemental Data. Error bars indicate standard error. Statistical significance was tested using Student's t test.

Experiments with Semliki Forest Virus

Generation of Semliki Forest Virus constructs, generation of virus stocks, and neuron infection were performed as published (Ashery et al., 1999).

Western Blotting

Antibodies and methods used for Western blotting are described in Supplemental Data. Protein levels in Western blots of Munc13-1 and bMunc13-2 were determined densitometrically by using ImageJ (National Institutes of Health). Expression levels were normalized using β-Tubulin as loading control. Error bars indicate standard error. Statistical significance was tested using Student's t test.

Supplemental Data

Supplemental Data include Supplemental Experimental Procedures, Supplemental References, and two figures and can be found with this article online at http://www.cell.com/cgi/content/full/131/4/796/DC1/.

ACKNOWLEDGMENTS

We thank A. Galinski, I. Thanhäuser, D. Schwerdtfeger, and the staff of the MPIEM Animal Facility for technical assistance. We are grateful to E. Neher for comments and discussions. This work was supported by the Max Planck Society and the German Research Foundation (Grant SFB406/A1 to N.B.).

Received: June 21, 2007
Revised: September 22, 2007
Accepted: November 1, 2007
Published: November 15, 2007

REFERENCES

Andrews-Zwilling, Y.S., Kawabe, H., Reim, K., Varoqueaux, F., and Brose, N. (2006). Binding to Rab3A-interacting molecule RIM regulates the presynaptic recruitment of Munc13–1 and ubMunc13–2. J. Biol. Chem. *281*, 19720–19731.

Ashery, U., Betz, A., Xu, T., Brose, N., and Rettig, J. (1999). An efficient method for infection of adrenal chromaffin cells using the Semliki Forest virus gene expression system. Eur. J. Cell Biol. *78*, 525–532.

Augustin, I., Rosenmund, C., Sudhof, T.C., and Brose, N. (1999). Munc13–1 is essential for fusion competence of glutamatergic synaptic vesicles. Nature *400*, 457–461.

Basu, J., Shen, N., Dulubova, I., Lu, J., Guan, R., Guryev, O., Grishin, N.V., Rosenmund, C., and Rizo, J. (2005). A minimal domain responsible for Munc13 activity. Nat. Struct. Mol. Biol. *12*, 1017–1018.

Beinfeld, M.C., Blum, A., Vishnuvardhan, D., Fanous, S., and Marchand, J.E. (2005). Cholecystokinin levels in prohormone convertase 2 knock-out mouse brain regions reveal a complex phenotype of region-specific alterations. J. Biol. Chem. *280*, 38410–38415.

Bekkers, J.M., and Stevens, C.F. (1991). Excitatory and inhibitory autaptic currents in isolated hippocampal neurons maintained in cell culture. Proc. Natl. Acad. Sci. USA *88*, 7834–7838.

Betz, A., Okamoto, M., Benseler, F., and Brose, N. (1997). Direct interaction of the rat unc-13 homologue Munc13–1 with the N terminus of syntaxin. J. Biol. Chem. *272*, 2520–2526.

Betz, A., Thakur, P., Junge, H.J., Ashery, U., Rhee, J.S., Scheuss, V., Rosenmund, C., Rettig, J., and Brose, N. (2001). Functional interaction of the active zone proteins Munc13–1 and RIM1 in synaptic vesicle priming. Neuron *30*, 183–196.

Cawley, N.X., Zhou, J., Hill, J.M., Abebe, D., Romboz, S., Yanik, T., Rodriguiz, R.M., Wetsel, W.C., and Loh, Y.P. (2004). The carboxypeptidase E knockout mouse exhibits endocrinological and behavioral deficits. Endocrinology *145*, 5807–5819.

Charlie, N.K., Schade, M.A., Thomure, A.M., and Miller, K.G. (2006). Presynaptic UNC-31 (CAPS) is required to activate the G alpha(s) pathway of the Caenorhabditis elegans synaptic signaling network. Genetics *172*, 943–961.

Dimova, K., Kawabe, H., Betz, A., Brose, N., and Jahn, O. (2006). Characterization of the Munc13-calmodulin interaction by photoaffinity labeling. Biochim. Biophys. Acta *1763*, 1256–1265.

Dulubova, I., Lou, X., Lu, J., Huryeva, I., Alam, A., Schneggenburger, R., Sudhof, T.C., and Rizo, J. (2005). A Munc13/RIM/Rab3 tripartite complex: from priming to plasticity? EMBO J. *24*, 2839–2850.

Furuta, M., Yano, H., Zhou, A., Rouille, Y., Holst, J.J., Carroll, R., Ravazzola, M., Orci, L., Furuta, H., and Steiner, D.F. (1997). Defective prohormone processing and altered pancreatic islet morphology in mice lacking active SPC2. Proc. Natl. Acad. Sci. USA *94*, 6646–6651.

Gracheva, E.O., Burdina, A.O., Holgado, A.M., Berthelot-Grosjean, M., Ackley, B.D., Hadwiger, G., Nonet, M.L., Weimer, R.M., and Richmond, J.E. (2006). Tomosyn inhibits synaptic vesicle priming in Caenorhabditis elegans. PLoS Biol. *4*, e261. 10.1371/journal.pbio.0040261.

Gracheva, E.O., Burdina, A.O., Touroutine, D., Berthelot-Grosjean, M., Parekh, H., and Richmond, J.E. (2007). Tomosyn negatively regulates CAPS-dependent peptide release at Caenorhabditis elegans synapses. J. Neurosci. *27*, 10176–10184.

Junge, H.J., Rhee, J.S., Jahn, O., Varoqueaux, F., Spiess, J., Waxham, M.N., Rosenmund, C., and Brose, N. (2004). Calmodulin and Munc13 form a Ca2+ sensor/effector complex that controls short-term synaptic plasticity. Cell *118*, 389–401.

Koch, H., Hofmann, K., and Brose, N. (2000). Definition of Munc13-homology-domains and characterization of a novel ubiquitously expressed Munc13 isoform. Biochem. J. *349*, 247–253.

Mahapatra, N.R., O'Connor, D.T., Vaingankar, S.M., Hikim, A.P., Mahata, M., Ray, S., Staite, E., Wu, H., Gu, Y., Dalton, N., et al. (2005). Hypertension from targeted ablation of chromogranin A can be rescued by the human ortholog. J. Clin. Invest. *115*, 1942–1952.

Maycox, P.R., Deckwerth, T., Hell, J.W., and Jahn, R. (1988). Glutamate uptake by brain synaptic vesicles. Energy dependence of transport and functional reconstitution in proteoliposomes. J. Biol. Chem. *263*, 15423–15428.

McEwen, J.M., Madison, J.M., Dybbs, M., and Kaplan, J.M. (2006). Antagonistic regulation of synaptic vesicle priming by Tomosyn and UNC-13. Neuron *51*, 303–315.

Morgan, A., and Burgoyne, R.D. (1997). Common mechanisms for regulated exocytosis in the chromaffin cell and the synapse. Semin. Cell Dev. Biol. *8*, 141–149.

Otsu, Y., and Murphy, T.H. (2004). Optical postsynaptic measurement of vesicle release rates for hippocampal synapses undergoing asynchronous release during train stimulation. J. Neurosci. *24*, 9076–9086.

Palmer, C.L., Cotton, L., and Henley, J.M. (2005). The molecular pharmacology and cell biology of alpha-amino-3-hydroxy-5-methyl-4-isoxazolepropionic acid receptors. Pharmacol. Rev. *57*, 253–277.

Pan, H., Che, F.Y., Peng, B., Steiner, D.F., Pintar, J.E., and Fricker, L.D. (2006). The role of prohormone convertase-2 in hypothalamic neuropeptide processing: a quantitative neuropeptidomic study. J. Neurochem. *98*, 1763–1777.

Pyott, S.J., and Rosenmund, C. (2002). The effects of temperature on vesicular supply and release in autaptic cultures of rat and mouse hippocampal neurons. J. Physiol. *539*, 523–535.

Renden, R., Berwin, B., Davis, W., Ann, K., Chin, C.T., Kreber, R., Ganetzky, B., Martin, T.F., and Broadie, K. (2001). Drosophila CAPS is an essential gene that regulates dense-core vesicle release and synaptic vesicle fusion. Neuron *31*, 421–437.

Rhee, J.S., Betz, A., Pyott, S., Reim, K., Varoqueaux, F., Augustin, I., Hesse, D., Sudhof, T.C., Takahashi, M., Rosenmund, C., and Brose, N. (2002). Beta phorbol ester- and diacylglycerol-induced augmentation of transmitter release is mediated by Munc13s and not by PKCs. Cell *108*, 121–133.

Richmond, J.E., Weimer, R.M., and Jorgensen, E.M. (2001). An open form of syntaxin bypasses the requirement for UNC-13 in vesicle priming. Nature *412*, 338–341.

Rosenmund, C., Clements, J.D., and Westbrook, G.L. (1993). Nonuniform probability of glutamate release at a hippocampal synapse. Science *262*, 754–757.

Rosenmund, C., Sigler, A., Augustin, I., Reim, K., Brose, N., and Rhee, J.S. (2002). Differential control of vesicle priming and short-term plasticity by Munc13 isoforms. Neuron *33*, 411–424.

Rosenmund, C., and Stevens, C.F. (1996). Definition of the readily releasable pool of vesicles at hippocampal synapses. Neuron *16*, 1197–1207.

Rupnik, M., Kreft, M., Sikdar, S.K., Grilc, S., Romih, R., Zupancic, G., Martin, T.F., and Zorec, R. (2000). Rapid regulated dense-core vesicle exocytosis requires the CAPS protein. Proc. Natl. Acad. Sci. USA *97*, 5627–5632.

Sadakata, T., Itakura, M., Kozaki, S., Sekine, Y., Takahashi, M., and Furuichi, T. (2006). Differential distributions of the Ca2+ -dependent activator protein for secretion family proteins (CAPS2 and CAPS1) in the mouse brain. J. Comp. Neurol. *495*, 735–753.

Sadakata, T., Kakegawa, W., Mizoguchi, A., Washida, M., Katoh-Semba, R., Shutoh, F., Okamoto, T., Nakashima, H., Kimura, K., Tanaka, M., et al. (2007). Impaired cerebellar development and function in mice lacking CAPS2, a protein involved in neurotrophin release. J. Neurosci. *27*, 2472–2482.

Sadakata, T., Mizoguchi, A., Sato, Y., Katoh-Semba, R., Fukuda, M., Mikoshiba, K., and Furuichi, T. (2004). The secretory granule-associated protein CAPS2 regulates neurotrophin release and cell survival. J. Neurosci. *24*, 43–52.

Schoch, S., Deak, F., Konigstorfer, A., Mozhayeva, M., Sara, Y., Sudhof, T.C., and Kavalali, E.T. (2001). SNARE function analyzed in synaptobrevin/VAMP knockout mice. Science *294*, 1117–1122.

Speese, S., Petrie, M., Shuske, K., Ailion, M., Ann, K., Iwasaki, K., Jorgensen, E.M., and Martin, T.F. (2007). UNC-31 (CAPS) is required for dense-core vesicle but not synaptic vesicle exocytosis in Caenorhabditis elegans. J. Neurosci. *27*, 6150–6162.

Speidel, D., Bruederle, C.E., Enk, C., Voets, T., Varoqueaux, F., Reim, K., Becherer, U., Fornai, F., Ruggieri, S., Holighaus, Y., et al. (2005). CAPS1 regulates catecholamine loading of large dense-core vesicles. Neuron *46*, 75–88.

Speidel, D., Varoqueaux, F., Enk, C., Nojiri, M., Grishanin, R.N., Martin, T.F., Hofmann, K., Brose, N., and Reim, K. (2003). A family of Ca2+-dependent activator proteins for secretion: comparative analysis of structure, expression, localization, and function. J. Biol. Chem. *278*, 52802–52809.

Stevens, C.F., and Tsujimoto, T. (1995). Estimates for the pool size of releasable quanta at a single central synapse and for the time required to refill the pool. Proc. Natl. Acad. Sci. USA *92*, 846–849.

Stevens, D.R., Wu, Z.X., Matti, U., Junge, H.J., Schirra, C., Becherer, U., Wojcik, S.M., Brose, N., and Rettig, J. (2005). Identification of the minimal protein domain required for priming activity of Munc13–1. Curr. Biol. *15*, 2243–2248.

Takamori, S., Holt, M., Stenius, K., Lemke, E.A., Gronborg, M., Riedel, D., Urlaub, H., Schenck, S., Brugger, B., Ringler, P., et al. (2006). Molecular anatomy of a trafficking organelle. Cell *127*, 831–846.

Tandon, A., Bannykh, S., Kowalchyk, J.A., Banerjee, A., Martin, T.F., and Balch, W.E. (1998). Differential regulation of exocytosis by calcium and CAPS in semi-intact synaptosomes. Neuron *21*, 147–154.

Varoqueaux, F., Sigler, A., Rhee, J.S., Brose, N., Enk, C., Reim, K., and Rosenmund, C. (2002). Total arrest of spontaneous and evoked synaptic transmission but normal synaptogenesis in the absence of Munc13-mediated vesicle priming. Proc. Natl. Acad. Sci. USA *99*, 9037–9042.

Walent, J.H., Porter, B.W., and Martin, T.F. (1992). A novel 145 kd brain cytosolic protein reconstitutes Ca(2+)-regulated secretion in permeable neuroendocrine cells. Cell *70*, 765–775.

Washbourne, P., Thompson, P.M., Carta, M., Costa, E.T., Mathews, J.R., Lopez-Bendito, G., Molnar, Z., Becher, M.W., Valenzuela, C.F., Partridge, L.D., and Wilson, M.C. (2002). Genetic ablation of the t-SNARE SNAP-25 distinguishes mechanisms of neuroexocytosis. Nat. Neurosci. *5*, 19–26.

Zhu, X., Zhou, A., Dey, A., Norrbom, C., Carroll, R., Zhang, C., Laurent, V., Lindberg, I., Ugleholdt, R., Holst, J.J., and Steiner, D.F. (2002). Disruption of PC1/3 expression in mice causes dwarfism and multiple neuroendocrine peptide processing defects. Proc. Natl. Acad. Sci. USA *99*, 10293–10298.

Zucker, R.S., and Regehr, W.G. (2002). Short-term synaptic plasticity. Annu. Rev. Physiol. *64*, 355–405.